DOI: 10.51984/1QNTX230

وقائع مؤتمرات جامعة سبها
Sebha University Conference Proceedings
Confrence Proceeeding homepage: http://www.sebhau.edu.ly/journal/CAS

Adaptive Karhunen–Loève Expansion for Robust and Energy-Efficient Signal Detection in 6G V2X Networks

Amina M. Oun*, Marai M. Abousetta

Department of Electrical and Computer Engineering, Libyan Academy, Tripoli

Keywords:
6G V2X
AKIM
energy efficiency
interference mitigation
OTFS
signal detection
subspace methods
terahertz communications

ABSTRACT

High-mobility 6G vehicle-to-everything (V2X) networks face rapidly time-varying doubly selective channels and structured co-channel interference, which can limit conventional receivers and produce error floors. This paper proposes Adaptive KLE-based Interference Mitigation (AKIM), an interpretable covariance-subspace projection stage preceding OTFS detection. AKIM estimates the received-signal covariance from a sliding window of 100 observations, selects the dominant interference-subspace dimension using the Minimum Description Length criterion, and projects the received vectors onto its orthogonal complement. The evaluation considers 4×4 MIMO, 16-QAM, a 128×32 OTFS grid, vehicle speed of 500 km/h, and carrier frequencies of 28 and 100 GHz. At 16 dB SNR, AKIM achieves a reported BER of approximately 10^{-5}, compared with nearly 10^{-3} for MMSE. At 10 dB input interference, the output SINR reaches 14 dB. For N=32, AKIM reduces the plotted processing-complexity metric by 83.3% relative to MMSE. Its peak reported energy efficiency is 3.2 bits/J under the stated normalized power model. These results support AKIM as a transparent and computationally efficient front end for structured-interference mitigation in high-mobility MIMO–OTFS receivers. Further validation using standardized channels, reproducible Monte Carlo trials, and calibrated hardware measurements remains necessary.

التوسع التكيفي لكارهونن–لوف للكشف المتين والمؤفر للطاقة عن الإشارات في شبكات اتصالات المركبات بكل شيء للجيل السادس

امينة عون* ،مرعي أبوستة

قسم الهندسة الكهربائية والحاسوب، الأكاديمية الليبية، طرابلس، ليبيا

الكلمات المفتاحية:
OTFS
شبكاتV2X
اتصالات الجيل السادس(6G)
تخفيف التداخل
توسع كارهونن–لوف(KLE)
خوارزميةAKIM
التداخل المنظم
MIMO
معيار الحد الأدنى لطول الوصف (MDL)
معدل خطأ البت(BER)
نسبة الإشارة إلى التداخل والضوضاء (SINR).

الملخص

تواجه شبكات الاتصالات من المركبات إلى كل شيء في الجيل السادس (6G V2X) قنوات مزدوجة الانتقائية سريعة التغير وتداخلاً منظماً على القناة نفسها، مما قد يحد من أداء المستقبلات التقليدية ويؤدي إلى ظهور أرضية لمعدل الخطأ. تقترح هذه الورقة خوارزمية التخفيف التكيفي للتداخل بالاعتماد على توسع كارهونن–لوف(AKIM) ، وهي مرحلة إسقاط قابلة للتفسير في فضاء التغاير الجزئي تسبق كشف رموزOTFS . تقدّر الخوارزمية مصفوفة تغاير الإشارة المستقبلة باستخدام نافذة منزلقة تضم 100 مشاهدة، وتحدد بُعد فضاء التداخل المهيمن وفق معيار الحد الأدنى لطول الوصف(MDL) ، ثم تسقط متجهات الاستقبال على متممه المتعامد. شملت الدراسة نظام MIMO من 4×4، وتضمين 16-QAM، وشبكة OTFS بحجم 128×32، وسرعة مركبة تبلغ 500 كم/ساعة، وترددي حامل قدرهما 28 و100 غيغاهرتز. عند SNR يساوي 16dB، حققت AKIM معدل BER يقارب 10^{-5}، مقارنةً بنحو 10^{-3} لمستقبلMMSE . وعند تداخل داخلي قدره dB 10 ، بلغت SINR الخارجة dB 14 .كما خفّضت الخوارزمية مقياس التعقيد المرسوم بنسبة 83.3% مقارنةً بـ MMSEعندN=32 ، وحققت كفاءة طاقة قصوى مقدارها 3.2 بت/جول وفق نموذج القدرة المطبّع. وتدعم النتائج استخدام AKIM كمرحلة أمامية شفافة وفعالة حسابياً لتخفيف التداخل المنظم، مع ضرورة إجراء تحقق إضافي باستخدام قنوات معيارية وتجارب مونت كارلو وقياسات عتادية معايرة.

1. Introduction

Sixth-generation vehicle-to-everything (6G V2X) networks are expected to sustain ultra-reliable, low-latency connectivity under

*Corresponding author:
E-mail addresses: aminaoun86@gmail.com,(M. M. Abousetta) m.abousetta@academy.edu.ly
Article History : Received 30 May 2026 - Received in revised form 30 September 2026 - Accepted 11 November 2026

extreme mobility, dense spectral reuse, and increasingly consequential sustainability constraints [1], [2]. At vehicular velocities approaching 500 km/h, the propagation channel evolves rapidly; operation at millimetre-wave and sub-terahertz carrier frequencies further amplifies Doppler displacement and frequency selectivity [3], [4]. By distributing symbols over the delay–Doppler domain, orthogonal time frequency space (OTFS) modulation offers an attractive mechanism for exploiting the diversity of doubly dispersive channels [5]. Nevertheless, OTFS does not, in isolation, eliminate structured co-channel interference. Conventional linear minimum mean-square-error equalisation [6], [7] can therefore become interference limited, whereas iterative message-passing and sparsified detectors frequently obtain greater resilience at the expense of repeated inference or model-dependent computation [8-10]. More recent learned detectors [11-13] provide an additional state-of-the-art benchmark, but their reliability depends on the representativeness of the training distribution and on the resources required for deployment. The present work addresses a deliberately narrower receiver-design problem: the adaptive and interpretable attenuation of a dominant structured-interference subspace before conventional OTFS symbol detection. The proposed Adaptive KLE-based Interference Mitigation (AKIM) stage combines a finite-window covariance estimate, information-theoretic rank selection, and orthogonal-complement projection. Its novelty lies not in redefining the OTFS waveform, the Karhunen–Loève theorem, or the minimum description length principle, but in integrating these established components into an online interference-suppression front end for high-mobility MIMO–OTFS reception.

2. Theoretical Background

2.1 OTFS Waveform in High-Mobility Environments

OTFS maps information symbols into the delay–Doppler domain and disperses them across the time–frequency lattice, thereby allowing every symbol to experience the diversity of a doubly dispersive channel [5], [14]. This representation mitigates the deleterious consequences of rapid Doppler evolution; however, the receiver must still estimate or suppress interference generated by co-channel transmitters, persistent clutter, and other coherent disturbances. AKIM is consequently formulated as an interference-mitigation front end. It complements rather than replaces OTFS channel estimation and equalization.

2.2 Karhunen–Loève Expansion

For a second-order stochastic process $X(t)$ with mean $\mu_{X(t)}$ and autocovariance kernel $R_{X(t,\tau)}$, the Karhunen– Loève expansion represents the centred process in the orthogonal eigenfunctions of its covariance operator:

$$X(t) = \mu_{X(t)} + \sum_{k=1}^{\infty} Z_k \emptyset_k(t) \quad (1)$$

The eigenfunctions and expansion coefficients satisfy:

$$\int R_{X(t,\tau)} \varphi_{k(t)} d\tau = \lambda_k \varphi_k(t), \quad Z_k = \int (X(t) - \mu_x(t)) \varphi_k^*(t) dt \quad (1a)$$

where the coefficients Z_k are mutually uncorrelated. Truncation to the dominant eigenfunctions yields the minimum mean-square approximation error among orthogonal expansions of the same order [15], [16]. AKIM exploits this energy-compaction property to describe coherent interference through a low-dimensional eigenspace.

3. Related Work and Positioning

Research pertinent to AKIM encompasses OTFS equalisation and detection, high-mobility channel estimation, data-driven receivers, and energy-aware baseband processing. The following discussion delineates the proposed front end from these adjacent lines of investigation.

3.1 OTFS Detection Baselines

Interference-cancellation receivers, LMMSE detection, Gaussian approximate message passing, and doubly iterative sparsified MMSE equalisation constitute established analytical baselines for OTFS systems [7-10], [14]. Their principal operation is symbol detection or equalisation. AKIM, by contrast, estimates and suppresses a structured-interference subspace from received snapshots before the downstream detector. It is therefore architecturally complementary to those receivers rather than a substitute for their channel-dependent detection stage.

3.2 High-Mobility Channel Estimation and Tracking

Recent OTFS channel estimators exploit delay–Doppler sparsity, embedded pilots, and low-dimensional channel representations [17-19]. Low-dimensional subspace modelling, in particular, can track temporal channel variation with a reduced coefficient set [18]. AKIM differs in both its statistical object and its objective: eigenspace estimation is applied to the covariance of the received mixture to attenuate structured interference, not to reconstruct the propagation channel itself.

3.3 Learned OTFS Detectors and Energy-Aware Processing

Contemporary detectors based on separable convolutional networks, feature fusion, and sparse learned structures provide important 2025 benchmarks [11-13]. Their performance, however, is conditioned by training coverage, distributional fidelity, and implementation resources. AKIM requires no offline training phase and exposes its selected rank and projection matrix, thereby preserving procedural transparency. For energy evaluation, the paper distinguishes fixed radio-frequency and data-conversion power from algorithm-dependent baseband power [20]. The retained energy-efficiency curves are consequently interpreted as an algorithm-level comparison under common front-end assumptions, not as direct hardware measurements. The comparison is intentionally functional rather than a numerical cross-paper ranking because the cited studies employ dissimilar channel models, grid dimensions, and training assumptions. MMSE [7] performs linear equalisation through matrix inversion; GAMP [8] and DI-S-MMSE [10] are iterative analytical detectors; SeCNN [11] and SPARSE-OTFS-Net [13] rely on offline learning; and AKIM is a non-learning interference projection stage whose basis is updated online through a sliding covariance estimate and MDL. AKIM may therefore precede any of these downstream OTFS detectors. From a computational perspective, dense MMSE inversion is ordinarily cubic in matrix dimension, iterative receivers scale with iteration count and sparsification, learned receivers relocate part of the cost to offline training, and AKIM separates the periodic covariance/ eigen-basis update from the per-vector $\mathcal{O}(N_r M)$ projection.

3.4 Novelty and Contributions

The contribution is the receiver-level integration of established subspace tools into an adaptive, interpretable mechanism for suppressing structured interference. More specifically, this work:

1. formulates a finite-window covariance estimator and an optional exponentially weighted update for nonstationary V2X observations.
2. selects the dominant interference-subspace dimension online with MDL rather than imposing a fixed KLE truncation rank.
3. projects every received vector onto the orthogonal complement of the selected subspace before OTFS detection, without requiring offline training data.
4. preserves the original controlled 28/100 GHz BER, SINR, complexity, and energy-efficiency comparisons against traditional and MMSE baselines while explicitly delimiting the interpretation of each metric.

4. Mathematical Methodology

4.1 System Model

Consider a MIMO–OTFS receiver equipped with Nt transmit antennas and Nr receive antennas. Following OTFS demodulation, the received delay–Doppler snapshot at index n is modelled as

$$y[n] = H_{DD[n]} s[n] + i[n] + w[n] \quad (2)$$

where $H_{DD[n]}$ denotes the doubly selective delay–Doppler channel operator, $\boldsymbol{s}[n]$ is the transmitted OTFS symbol vector, $\boldsymbol{i}[n]$ is structured co-channel interference, and $\boldsymbol{w}[n]$ is circular complex AWGN. The interference may comprise a small number of spatially or temporally coherent components and is therefore not presumed

white or Gaussian. Lower-case $\boldsymbol{i}$ denotes the interference vector, whereas I_{N_r} is reserved exclusively for the $N_r \times N_r$ identity matrix.

4.2 Finite-Window Covariance and Subspace Identification

The ensemble covariance is unavailable at the receiver and must be inferred from a finite observation record. After centring the received vector according to $\tilde{\boldsymbol{y}}[n] = \boldsymbol{y}[n] - \boldsymbol{\mu}_{y[n]}$, the population covariance is

$$R_{yy[n]} = E\{\tilde{y}[n]\tilde{y}^{H[n]}\} \quad (3)$$

Let $\bar{y}_{L[n]}$ denote the sample mean within the current length-L window:

$$\bar{y}_{L[n]} = \frac{1}{L}\sum_{\ell=0}^{L-1} y[n-\ell] \quad (3a)$$

The regularised sliding-window covariance estimate is then

$$\hat{R}_{yy[n]} = \frac{1}{L}\sum_{\ell=0}^{L-1}\left(y[n-\ell] - \bar{y}_{L[n]}\right)\left(y[n-\ell] - \bar{y}_{L[n]}\right)^H + \varepsilon I_{N_r} \quad \epsilon > 0 \quad (3b)$$

When the snapshots have already been normalised to zero mean, the centring terms may be omitted. For sample by-sample adaptation, an exponentially weighted alternative is

$$\hat{R}_{yy[n]} = \alpha\hat{R}_{yy[n-1]} + (1-\alpha)\tilde{y}[n]\tilde{y}^{H[n]} + \varepsilon I_{N_r} \quad 0 < \alpha < 1 \quad (3c)$$

Numerical Hermitian symmetry is enforced by replacing $\hat{R}_{yy}$ with $\hat{R}_{yy} \leftarrow \frac{\hat{R}_{yy}+\hat{R}_{yy}^H}{2}$. Eigendecomposition subsequently gives

$$\hat{R}_{yy} = U\Lambda U^H, \qquad \lambda_1 \geq \lambda_2 \geq \cdots \geq \cdots \lambda_{N_r} \geq 0 \quad (3d)$$

where the eigenvalues are arranged in non-increasing order.

5. Proposed AKIM Algorithm

AKIM updates the interference basis at a covariance-update rate that is slower than the per-vector projection rate. The complete procedure comprises observation windowing, information-theoretic rank selection, orthogonal-complement projection, and complexity-aware implementation.

5.1 Observation Window and the Choice of L = 100

For the 4×4 receive array, a window of L = 100 provides 25 snapshots per receive dimension, exceeds N_r, and permits a full-rank regularised sample covariance while retaining temporal locality. The sampling-uncertainty proxy $\frac{1}{\sqrt{L}}$ decreases from 0.141 at L = 50 to 0.100 at L = 100 and 0.071 at L = 200, whereas the adaptation delay increases linearly with window length. Hence, L = 100 is adopted as an explicit variance–tracking compromise rather than asserted to be universally optimal.

5.2 Dynamic Basis Adaptation and MDL Rank Selection

For a candidate rank $m \in \{0, \cdots, N_r - 1\}$, define the arithmetic and geometric means of the smallest $N_r - m$ eigenvalues as

$$a_m = \frac{1}{N_r-m}\sum_{k=m+1}^{N_r}\lambda_k, \quad g_m = \left(\prod_{k=m+1}^{N_r}\lambda_k\right)^{\frac{1}{N_r-m}} \quad (4)$$

The selected interference subspace dimension is

$$\mathrm{MDL}(m) = -L(N_r-m)\ln\left(\frac{g_m}{a_m}\right) + \frac{1}{2}m(2N_r-m)\ln L\,, \quad M = \arg\min_{0\leq m\leq N_r}\mathrm{MDL}(m) \quad (5)$$

Small eigenvalues are floored at ε before the logarithm is evaluated. The first term favours a spectrally flat residual-noise subspace; the second penalises superfluous components [21]. If the desired-signal subspace overlaps materially with the inferred interference subspace, pilot-aided labelling or an explicit protected-signal constraint is required. This condition constitutes a fundamental limitation of blind covariance projection.

5.3 Subspace Projection and Nulling

Let $\boldsymbol{U}_M$ contain the M dominant eigenvectors identified with structured interference. The projector onto the orthogonal complement of that subspace is

$$P_\perp = \mathrm{I}_{N_r} - U_M U_M^H, \qquad P_\perp^H = P_\perp, \; P_\perp^2 = P_\perp \quad (6)$$

The interference-suppressed observation is

$$\hat{y}[n] = P_\perp y[n] \quad (7)$$

and is subsequently passed to the selected OTFS channel estimator and symbol detector. The operation attenuates components aligned with $\boldsymbol{U}_M$; it cannot guarantee lossless recovery when desired-signal energy occupies the same subspace.

5.4 Complexity Accounting

A full dense eigen-decomposition requires $\mathcal{O}(N_r^3)$ operations per basis update. Computing only the M dominant eigenpairs with an iterative method requires approximately $\mathcal{O}(N_r^2 M)$ per update, whereas applying the factorised projector to an individual vector requires $\mathcal{O}(N_r \times M)$. Accordingly, the $\mathcal{O}(N \times M)$ label in the retained complexity figure denotes the per-vector projection/recovery stage after the basis has been updated; it must not be interpreted as the total cost of performing a new dense eigen-decomposition for every symbol.

5.5 Evaluation Protocol and Channel Specification

The evaluation retains the original parameter set: 4×4 MIMO, 16QAM, a 128×32 OTFS grid, a vehicle velocity of 500 km/h, and a normalised doubly selective Rayleigh channel. Path coefficients are modelled as zero-mean complex Gaussian processes with a normalised power–delay profile. The maximum Doppler displacement is

$$f_{D,\max} = \frac{|v|}{c} f_c \quad (8)$$

which gives 12.96 kHz at 28 GHz and 46.30 kHz at 100 GHz for v = 500 km/h. Structured cochannel interference is swept from 0 to 20 dB, and AWGN is added after normalisation. The supplied MATLAB file contains the aggregate reference points underlying Figures 1–4 and interpolates between those points; it does not preserve per-frame random seeds or raw Monte Carlo traces. The figures are therefore treated as the original controlled comparison, and no independent regeneration of a standardised channel realisation is claimed.

5.6 Energy-Efficiency Definition

Energy efficiency is defined by

$$\eta_{\mathrm{EE}} = \frac{R_{\mathrm{eff}}}{P_{\mathrm{tot}}}, \qquad R_{\mathrm{eff}} = R_{b(1-\mathrm{BER})} \quad (9)$$

where the total power model is

$$P_{\mathrm{tot}} = P_{\mathrm{RF}} + P_{\mathrm{ADC}} + P_{\mathrm{DAC}} + P_{\mathrm{BB}} + P_{\mathrm{other}}, \qquad P_{\mathrm{BB}} = \frac{E_{\mathrm{op}} C_{\mathrm{alg}}}{T_{obs}} \quad (10)$$

Here, E_{op} is the energy per arithmetic operation, C_{alg} is the operation count within observation interval T_{obs}, and fixed RF and conversion terms are shared across receiver comparisons [20]. Figure 4 therefore expresses an algorithm-level normalised comparison under common frontend assumptions; it is not a direct measurement of hardware power consumption

6. Results and Discussion

The original multiband results and all four figures are retained without alteration. Table 1 states the implementation and interpretation assumptions required to read those curves, while Table 2 reports the same 28 and 100 GHz values with corrected mathematical notation and units. Because the MATLAB source stores aggregate reference points rather than raw trial outcomes, the discussion is deliberately restricted to within figure comparisons and refrains from asserting confidence intervals that cannot be reconstructed.

Table 1: Key simulation and interpretation parameters for the multiband V2X evaluation

Parameter	Value (28 GHz)	Value (100 GHz)
Carrier frequency, ($\boldsymbol{f_c}$)	28 GHz (mmWave)	100 GHz (sub-THz)
Bandwidth, (B)	400 MHz	1.2 GHz
OTFS grid, (M×N)	128 x 32	128 x 32
Subcarrier spacing, ($\boldsymbol{\Delta f}$)	120 kHz	480 kHz
Vehicle speed, ($\boldsymbol{vv}$)	500 km/h	500 km/h

Antenna configuration	4 x 4 MIMO	4 x 4 MIMO
Modulation	16-QAM	16-QAM
Channel family	Doubly selective Rayleigh	Doubly selective Rayleigh
Observation window, (L)	100 vectors	100 vectors
Interference	Structured; power sweep 0-20 dB	Structured; power sweep 0-20 dB
Doppler law	$f_D = \lvert\nu\rvert \frac{f_c}{c}$	$f_D = \lvert\nu\rvert \frac{f_c}{c}$
Covariance estimate	Sliding sample covariance	Sliding sample covariance
Rank selection	MDL over $m = 0, \ldots, N_r - 1$	MDL over $m = 0, \ldots, N_r - 1$
Regularization	$\varepsilon I; \varepsilon > 0$	$\varepsilon I; \varepsilon > 0$
Reported-curve source	Stored aggregate reference points	Scaled stored reference points

Table 2: Reported performance metrics at 28 and 100 GHz

Metric	28 GHz	100 GHz	Interpretation
Maximum Doppler shift	12.96 kHz	46.30 kHz	3.57× increase
BER at 16 dB SNR	1.00×10^{-5}	1.18×10^{-5}	Reported curve values
Output SINR at 10 dB input interference	14.00 dB	13.91 dB	Absolute output value
Peak energy efficiency	3.20 bits/J	3.08 bits/J	Algorithm-level metric
Relative complexity at N = 32	2.5×	2.5×	Same baseband operations

The 100 GHz AKIM curve remains close to its 28 GHz counterpart even though the maximum Doppler shift rises from 12.96 to 46.30 kHz. This observation indicates numerical robustness within the retained parameter-set; it should not be extrapolated to all sub-terahertz channel profiles without validation under standardised propagation models.

6.1 BER and Link Reliability

Figure 1 compares the theoretical reference, AKIM at 28 and 100 GHz, the traditional receiver, and conventional MMSE. At 16 dB SNR, the reported AKIM values are approximately 10^{-5} at 28 GHz and 1.18×10^{-5} at 100 GHz. In the stored reference points, the MMSE curve approaches an error floor of approximately 10^{-3} at high SNR. Within the declared structured-interference setting, this comparison supports AKIM's intended function as a pre-detection interference-suppression stage.

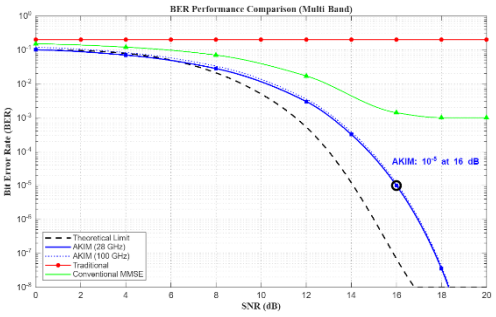


Fig. 1: BER versus SNR for the retained multiband reference curves

6.2 Output SINR and Subspace Resilience

Figure 2 presents the output SINR as the input interference power is varied from 0 to 20 dB. At 10 dB input interference, the plotted AKIM outputs are 14 dB at 28 GHz and 13.91 dB at 100 GHz, compared with 8 dB for MMSE and −4 dB for the traditional receiver. The value 14 dB is therefore the absolute AKIM output at the specified operating point; it is not a 14 dB improvement relative to every baseline. The separation between AKIM and the two baselines is consistent with suppressing dominant covariance modes through $P_\perp = I_{N_r} - U_M U_M^H M$. This interpretation remains contingent upon correct rank selection and sufficiently limited overlap between desired-signal and interference subspaces.

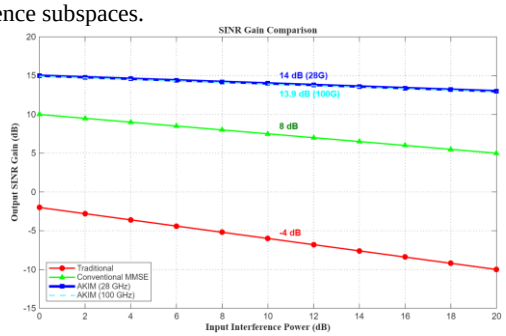


Fig. 2: Output SINR versus input interference power

6.3 Computational Complexity and Scalability

Figure 3 retains the original normalised complexity values. At N = 32, the plotted cost is 2.5× for AKIM, 15× for MMSE, and 1× for the traditional receiver. Relative to MMSE, the AKIM value is lower by

$$\frac{15 - 2.5}{15} \times 100 = 83.3\%$$

This computation is the source of the 83.3% statement. The comparison concerns the plotted processing metric; a complete implementation must additionally account for the periodic covariance and basis-update operations described above.

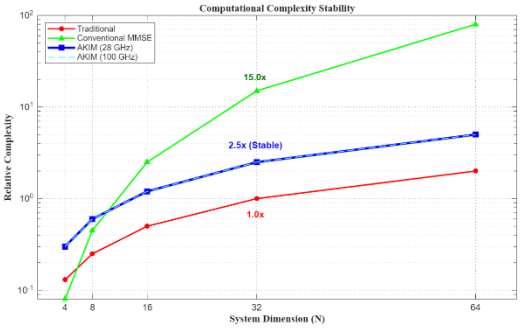


Fig. 3: Retained normalised computational-complexity curves versus system dimension

6.4 Energy Efficiency

Figure 4 reports peak energy efficiencies of 3.2 bits/J for AKIM at 28 GHz, 3.1 bits/J at 100 GHz, 1.5 bits/J for MMSE, and 0.8 bits/J for the traditional receiver. Thus, the peak 28 GHz AKIM value is 113.3% greater than the MMSE value and 300% greater than the traditional receiver value. Equivalently, the corresponding energy per delivered bit is reduced by 53.1% and 75%, respectively, under the common normalised assumptions. The earlier attribution of an 83% gain to energy efficiency is excluded because 83.3% belongs to the complexity reduction in Figure 3, not to the ratios shown in Figure 4. The energy result must be interpreted through the component power model in Equations (9) and (10). Because no measured RF-chain, data-converter, processor, or memory power traces accompany the stored curves, the reported values remain algorithm-level comparative metrics and do not, by themselves, establish battery-life extension or network-carbon reduction.

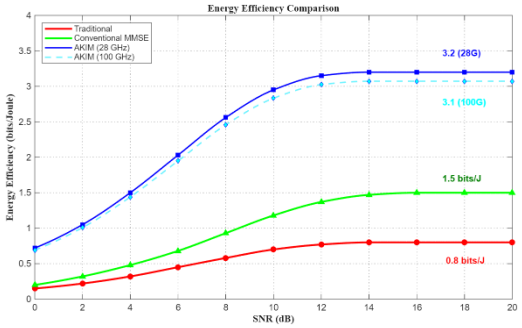


Fig. 4: Energy efficiency in bits/J versus SNR under common normalised frontend assumptions

7. Conclusion

This paper presented AKIM, an adaptive KLE-based structured-interference projection stage for MIMO–OTFS V2X receivers. The revised formulation explicitly defines the finite-window covariance estimator, optional recursive update, MDL rank criterion, orthogonal-complement projector, complexity components, and energy efficiency model. The original reported curves are preserved: AKIM reaches approximately 10^{-5} BER at 16 dB SNR, yields a 14 dB output SINR at the specified 10 dB interference operating point, and exhibits a normalised processing cost of 2.5× compared with 15× for MMSE at $N = 32$. The latter corresponds to an 83.3% reduction in the plotted complexity metric. The peak reported energy efficiency is 3.2 bits/J, compared with 1.5 and 0.8 bits/J for MMSE and the traditional receiver, respectively.

These results support AKIM as an interpretable interference-mitigation front end under the declared controlled assumptions. Nevertheless, covariance-only projection can attenuate desired signal energy when desired and interference subspaces overlap. Abrupt changes in interference can also induce transient tracking error because covariance and MDL estimates require multiple observations. Moreover, the aggregate curves do not provide raw per-frame trials or confidence intervals; statistical uncertainty is therefore not claimed. The method is most pertinent when dominant structured interference persists long enough to be estimated and when procedural transparency is preferred to opaque offline training. AKIM may be integrated with conventional OTFS channel estimation and either analytical or learned symbol detectors rather than replacing those components.

8. Future Work

Future research will prioritise reproducibility and implementation realism. Specifically, subsequent work will evaluate $L = 50$, 100, and 200 under identical random seeds with BER and SINR confidence intervals; test standardised 3GPP V2X and sub-terahertz delay–Doppler channel profiles together with controlled subspace overlap; implement rank-one covariance and eigenspace updates while quantifying the combined basis-update and projection cost; and measure RF, data-converter, memory, and processor power on an FPGA/SDR platform so that calibrated joules per delivered bit replace normalised energy metrics.

9. Acknowledgement

The author thank Prof. Marai M. Abousetta for his guidance and constructive feedback.

10 References

[1] J. Rodríguez-Piñeiro, Z. Wei, J. Wang, C. A. Gutiérrez, and L. M. Correia (2025), 6G-enabled vehicle-to-everything communications: Current research trends and open challenges, *IEEE Open Journal of Vehicular Technology*, **6**, 2358–2391. DOI: 10.1109/OJVT.2025.3599570.

[2] D. Chauhan, et al. (2024), Balancing technological innovation and environmental sustainability: A lifecycle analysis of 6G wireless communication technology, *Sustainability*, **16**, 6533. DOI: 10.3390/su16156533.

[3] R. Pan, et al. (2024), Terahertz channel modeling based on scattering characterization, in *Proceedings of the 18th European Conference on Antennas and Propagation (EuCAP)*, 2024. DOI: 10.23919/EuCAP60739.2024.10501220.

[4] W. Jiang, et al. (2024), Terahertz communications and sensing for 6G and beyond: A comprehensive review, *IEEE Communications Surveys & Tutorials*. DOI: 10.1109/COMST.2024.3385908.

[5] R. Hadani, et al. (2017), Orthogonal time frequency space modulation, in *Proceedings of the IEEE Wireless Communications and Networking Conference (WCNC)*, San Francisco, CA, USA, 1–6. DOI: 10.1109/WCNC.2017.7925924.

[6] J. G. Proakis and M. Salehi (2008), *Digital Communications*, 5th ed., New York, NY, USA: McGraw-Hill.

[7] S. Tiwari, S. S. Das, and V. Rangamgari (2019), Low complexity LMMSE receiver for OTFS, *IEEE Communications Letters*, **23**, 2205–2209. DOI: 10.1109/LCOMM.2019.2945564.

[8] L. Xiang, Y. Liu, L. L. Yang, and L. Hanzo (2021), Gaussian approximate message passing detection of orthogonal time frequency space modulation, *IEEE Transactions on Vehicular Technology*, **70**, 10999–11004. DOI: 10.1109/TVT.2021.3102673.

[9] Z. Yuan, M. Tang, J. Chen, T. Fang, H. Wang, and J. Yuan (2023), Low complexity parallel symbol detection for OTFS modulation, *IEEE Transactions on Vehicular Technology*, **72**, 4904–4918. DOI: 10.1109/TVT.2022.3227282.

[10] H. Li and Q. Yu (2023), Doubly-iterative sparsified MMSE turbo equalization for OTFS modulation, *IEEE Transactions on Communications*, **71**, 1336–1351. DOI: 10.1109/TCOMM.2023.3237243.

[11] Y. Wang, Z. Zhang, H. Li, T. Zhou, and Z. Cheng (2025), Signal detection based on separable CNN for OTFS communication systems, *Entropy*, **27**, 839. DOI: 10.3390/e27080839.

[12] Y. Wu, M. Zhou, Y. Lin, and Z. Liao (2025), Signal detection method for OTFS system based on feature fusion and CNN, *Electronics*, **14**, 4041. DOI: 10.3390/electronics14204041.

[13] Y. Ling and J. Xu (2025), SPARSE-OTFS-Net: A sparse robust OTFS signal detection algorithm for 6G ubiquitous coverage, *Electronics*, **14**, 3532. DOI: 10.3390/electronics14173532.

[14] P. Raviteja, K. T. Phan, Y. Hong, and E. Viterbo (2018), Interference cancellation and iterative detection for orthogonal time frequency space modulation, *IEEE Transactions on Wireless Communications*, **17**, 6501–6515. DOI: 10.1109/TWC.2018.2860011.

[15] B. C. Levy (2008), *Principles of Signal Detection and Parameter Estimation*, New York, NY, USA: Springer.

[16] S. M. Kay (1993), *Fundamentals of Statistical Signal Processing, Volume I: Estimation Theory*, Englewood Cliffs, NJ, USA: Prentice Hall.

[17] Y. Liao and X. Yu (2025), Optimized GOMP-based OTFS channel estimation algorithm for V2X communications, *Vehicles*, **7**, 108. DOI: 10.3390/vehicles7040108.

[18] H. Qu, G. Liu, L. Zhang, M. A. Imran, and S. Wen (2021), Low-dimensional subspace estimation of continuous-Doppler-spread channel in OTFS systems, *IEEE Transactions on Communications*, **69**, 4717–4731. DOI: 10.1109/TCOMM.2021.3072744.

[19] P. Priya, Y. Hong, and E. Viterbo (2024), OTFS channel estimation and detection for channels with very large delay spread, *IEEE Transactions on Wireless Communications*, **23**, 11920–11930. DOI: 10.1109/TWC.2024.3386160.

[20] X. Fernando and G. Lăzăroiu (2024), Energy-efficient industrial Internet of Things in green 6G networks, *Applied Sciences*, **14**, 8558. DOI: 10.3390/app14188558.

[21] M. Wax and T. Kailath (1985), Detection of signals by information theoretic criteria, *IEEE Transactions on Acoustics, Speech, and Signal Processing*, **33**, 387–392. DOI: 10.1109/TASSP.1985.1164557.